Seismic behaviour of concrete-filled steel tubular columns with internal H-section steel under pure torsion and compression–torsion loads

DOI:
10.1016/j.engstruct.2020.110761

Citation for published version (APA):
Pi, Z., Su, M., Peng, Y., Wang, Y., Luo, W., & Lan, Y. (2020). Seismic behaviour of concrete-filled steel tubular columns with internal H-section steel under pure torsion and compression–torsion loads. *Engineering Structures*, *216*, 110761. https://doi.org/10.1016/j.engstruct.2020.110761

Published in:
Engineering Structures

Pi, ZB, Su, M.N., Peng, Y.Y., Wang, Y.H., Luo, W., Lan, Y.S. (2020), "Seismic behaviour of concrete-filled steel tubular columns with internal H-section steel under pure torsion and compression–torsion loads", Engineering Structures, 216: 110761.

Seismic behaviour of concrete-filled steel tubular columns with internal H-section steel under pure torsion and compression–torsion loads

Zheng-Bo Pi[a], Meni Su[b], Yuan-yuan Peng[c], Yu-Hang Wang[a,d,*], Wei Luo[e], Yong-Sen Lan[e]

[a] School of Civil Engineering, Chongqing University, Chongqing, China

[b] School of Mechanical, Aerospace & Civil Engineering, Manchester University, Manchester, UK

[c] Department of Capital Construction and Planning, Chongqing University, Chongqing, China

[d] Key Laboratory of New Technology for Construction of Cities in Mountain Area (Chongqing University), Ministry of Education, Chongqing, China

[e] CSIC HaiZhuang Wind Power Co., Ltd., Chongqing, China

Abstract: Concrete-filled steel tube (CFST) columns have been widely used in the construction industry because of their excellent compression capacity and torsion resistance. Regarding traditional CFST columns, the H-CFST column with an additional H-section steel member embedded in the core concrete provides improved fire and compression resistance. In this study, the seismic performance of nine H-CFST columns under cyclic torsional and compression–cyclic torsional loads was experimentally analysed. In the experiments, the failure mode, torque versus torsional angle hysteresis, torque versus torsional angle skeleton, torsional stiffness degradation, and energy dissipation capacity were determined. The hysteretic curves of the H-CFST columns under torsion were relatively plump in shape and exhibited no 'pinching' phenomenon, and the torsional stiffness of the H-CFST columns under unloading and reverse loading was approximately equal to the initial torsional stiffness. In addition, the applied compression had remarkable effects on the torsional capacity, torsional ductility, torsional stiffness, and hysteretic loop energy dissipation of the H-CFST columns. The shear capacities of the steel and concrete under normal stress or combined normal and shear stress were firstly determined based on the latest theories and test results. Moreover, design method for the determination of the torsional capacity of H-CFST columns under compressive torsion is proposed based on the test results, and the theoretical contribution ratio of the H-section steel, steel tube, and concrete in the H-

CFST columns to the torsional capacity was determined.

Keywords: Compressive torsional capacity; Concrete-filled steel tube columns; Energy dissipation capacity; Seismic behaviour; Torsional behaviour; Torsional stiffness degradation.

∗ Corresponding authors: wangyuhang@cqu.edu.cn (Y. H. WANG)

1. Introduction

Concrete-filled steel tube (CFST) columns with internal H-section steel (H-CFST) are a new type of structural component; they are composed of an outer steel tube with an inner H-section steel member and concrete and are classified into concrete-filled circular steel tubes with embedded internal H-section steel (H-CFCSTs) and concrete-filled rectangular steel tubes with embedded internal H-section steel (H-CFRSTs). The key advantages of H-CFST columns over CFST columns are the improved fire protection, torsion resistance, and anti-buckling ability due to the internal welded steel members.

Few researchers have experimentally and numerically studied the behaviour and capacities of reinforced concrete (RC) and composite columns under combined loads. Prakash et al. investigated the behaviour of RC columns under bending and torsion with low and moderate shear stresses in the early compression stage [1]. The researchers concluded that the aspect ratio changes significantly the failure mode and deformation characteristics of RC columns. Circular CFSTs with different diameter-to-thickness ratios under compression were investigated by Wang et al. [2], who established a size-related model to estimate the bearing capacity of the large-size CFST columns under compression. Moreover, extensive experimental, numerical, and theoretical investigations of the behaviour of CFST columns under bending, compression, shear, torsion, and fire were conducted by Han [3], Elchalakani and Zhao [4], Wang [5], Wang et al. [6-7], Nie et al. [8], Beck and Kiyomiya [9]. The researchers mainly investigated the torsional capacity with the finite-element method based on their experimental results. In addition, steel and concrete composite columns with different forms have been investigated by researchers. For instance, Li et al. [10] studied concrete-encased CFST columns and developed finite-element models to analyse the behaviour of these new structural members under compression and torsion. Ding et al. [11] developed and investigated steel-RC-filled square steel tubular stub columns with experiments and numerical simulations, and concrete-filled double-skin steel tube columns were studied by Elchalakani et al. [12], Wang et al. [13], Elchalakani et al. [14], Farahi et al. [15], Ekmekyapar and Hasan [16-17], and Huang et al. [18-19]. The loading conditions considered in these experiments included axial compression and torsion. Recently, Shi [20] analysed the shear behaviour of H-CFST columns with square, circular, and rectangular external tubes through tests and finite-element analyses and revealed their failure modes and mechanical properties under shear: the shear capacity decreases with increasing shear span ratio. According to the available studies of concrete–steel composite columns in literature, the seismic behaviour of H-CFST columns under torsion and compressive torsion has not been investigated. However, when H-CFST columns are used as piers of curved girder bridges or side columns of multi-tower structures and bridge towers of suspension bridges, they are subjected to torsion and compression–torsion under earthquakes. This is because the stiffness centre and mass centre of curved girder bridges and multi-tower structures are not concentric, and the mass distribution of suspension bridges is unbalanced. Thus, the seismic behaviour of such new structural members must be investigated.

This is the first study to investigate the seismic performance of this new type of H-CFST columns under cyclic torsional and compression–cyclic torsional loads experimentally and thereafter proposed the design methods. First, this paper presents the experimental programme comprising the tests on three creative H-CFST short columns under pure torsion and six newly H-CFST long columns under pure torsion and compression–torsion loads. It is described how the horizontal loads, horizontal displacement, and vertical loads were applied to the specimens. In this study, the failure mode, the torque versus torsional angle hysteresis, torque versus torsional angle skeleton, torsional stiffness degradation, and energy dissipation capacities of the tested composite columns were determined and analysed. Moreover, the shear capacity of the steel and concrete under pure shear stress or especially combined normal and shear stress conditions was firstly deduced and validated against the previous tested dates, and a design method for predicting the torsional capacities of H-CFST columns on pure torsion and compression–torsion loads was assessed based on the test results and the deduced shear capacity of this paper.

2. Experimental programme

2.1 Test specimens

The nine H-CFST columns for the experimental tests are composed of a circular or rectangular tube, an internal welded H-section steel profile member, and concrete (Fig. 1). The internal H-section steel member was welded to the top and bottom plates by gas shielded welding, and the concrete was casted into the tube through two holes in the top plate. Two of the nine test specimens are H-CFST columns with an outer circular tube (diameter of 159 mm); four are H-CFCST columns with an outer circular tube (diameter of 219 mm); and three are H-CFRST columns with an outer rectangular tube (dimension of 200 mm). In addition, all steel tubes are seamless. The mix proportions of the concrete are 1: 2.29: 0.92: 0.38 (cement: stone: sand: water (by weight)), the slump value is 84 mm, and the average 28-day compressive strength of concrete is 40.7 MPa. Note that in the study, the authors have made an effort to minimize the shrinkage cracking by: (1) employing a small water-cement ratio (0.35), and (2) pouring concrete into steel tubes twice (i.e. casting the full steel tube at the first time, and filling the gaps after an hour at the second time).

The dimensions of the H-CFST columns are shown in Fig. 1, the loading information and configuration are listed in Table 1, and the material properties of the steel tubes and H-section steel member are provided in Table 2.

2.2 Test set-up and loading method

To apply cyclic torsion and compression–torsion loads to the H-CFST columns, a loading device was designed and fabricated (Fig. 2). As shown in Fig. 2(c), the base is a box-shaped steel structure fixed to the RC floor by high-strength anchor rods. The top and bottom plates of the columns are connected to the rigid girder and steel base by high-strength bolts. In addition, one end of the horizontal actuator or horizontal rigid link is connected to the rigid girder through a cross hinge, which can be freely rotated in the horizontal and vertical planes; the other end is attached to the connecting steel plate which is fixed to the RC shear wall. Two load cells were used to measure the applied loads with horizontal and vertical actuators. The cyclic torsion was applied (Fig. 2(d)) by the horizontal actuator and the compression load (Fig. 2(e)) by the vertical actuator. The displacements of the H-CFST columns were measured by three linear variable differential transformers (LVDTs): LVDT1 for the horizontal actuator and LVDT2 and LVDT3 for the vertical rigid girder, as shown in Fig. 3.

Furthermore, cyclic loading (Fig. 4(a)) with equal increments in the torsional angle was applied by controlling the horizontal displacement because the torsional angle and horizontal displacement exhibit linear correlation. The increments in the torsional angle ($\Delta\theta$) of specimens CH1-T, CH2-T, and RH–T were ±1.29°, ±1.72°, and ±1.72°, and the increments in the torsional angle ($\Delta\theta$) of specimens CH1-CT1, CH2-CT1, CH2-CT2, and RH-CT2 were ±0.65°, ±0.86°, ±0.86°, and ±0.86°, respectively. The constant compression load (Table 1 and Fig. 4(b)) was first applied to specimens CH1-CT1, CH2-CT1, CH2-CT2, and RH-CT2, and the displacement was controlled with a loading rate of 4 mm/min. When the minimal or maximal torsion angle was reached in each loading loop, the loading process was paused for one minute. Moreover, the process was stopped, and the specimens were unloaded when they were damaged. All displacement and load data of the columns were collected by an automatic data acquisition system. The maximal applied compression load (N) was below $0.48N_u$ for the H-CFCST columns (N_{u} is the measured compressive capacity of the column; Table 1), and the maximal applied compression load (N) was below $0.4N_u$ for the H-CFRST columns. Therefore, the conclusions depend on these conditions.

3. Test results and analysis

3.1 Failure modes

The failure modes of the H-CFST columns under cyclic torsional load in Fig. 5 are 90° X-shaped cracking with concrete crushing at the same location (Fig. 5(a)), and the H-CFCST columns exhibit 90° X-shaped uplifts on the external circular steel tube with concrete crushing (Fig. 5(b)); the H-CFRST column exhibits multiple 90° X-shaped cracks at the mid-height of the external rectangular steel tube and 90° X-shaped crushing failure in the concrete at the same location (Fig. 5(c)). Pure shear stress acted on the external steel tube, internal concrete, and H-section wielding steel when the cyclic torsional load was applied to the H-CFST columns. According to the *Mohr's circle-plane stress* and maximal in-plane shear stress [21], the direction of the principal maximal normal stress is 45° clockwise with respect to the horizontal axis. This led to the cracking of the internal concrete and external steel tube along the direction of the minimal normal stress (i.e. 135° clockwise with respect to the horizontal axis).

The failure modes of the H-CFST columns under compression are shown in Fig. 6; the H-CFCST and H-CFRST columns exhibit overall vertical buckling, and the H-CFRST column shows horizontal buckling on its top.

The failure modes of the H-CFST columns under combined compression and cyclic torsional load are shown in Fig. 7; the H-CFCST column with a diameter of 159 mm (CH1-CT1) exhibits overall buckling (Fig. 8(a)); the H-CFCST columns with sectional diameters of 219 mm (CH2-CT1 and CH2-CT2) exhibit overall buckling, oblique cracking on the concrete at the same location of the uplifts of the steel tube, and overall and local buckling on the flanges and webs of the H-section steel member (Figs. 7(b) and (c)); moreover, the H-CFRST column exhibits multiple 90° X-shaped cracks at the mid-height and both ends of the external steel tube, X-shaped cracks on the concrete at the same location, and overall and local buckling of the internal H-section steel member (Fig. 7(d)). This is because shear and normal stresses acted on the H-CFST columns when the static compression and cyclic torsion loads were applied. However, different from the results of the pure cyclic torsion load, the cracks of the concrete caused by the direction of the principal maximal normal stress are located at an angle below 45° clockwise with respect to the horizontal axis [21].

3.2 Torque versus torsional angle hysteresis loops

The torque versus torsional angle hysteresis loops of the H-CFST columns under cyclic torsional load are shown in Fig. 8. They exhibit a plump shape without a significant ‘pinching’ phenomenon. The unloading and reverse loading stiffness values are approximately equal to the initial elastic stiffness, and their degeneration is small. According to [21], the ‘effective lengths’ of the H-section steel and steel tube decrease when fixed or supported by in-filled concrete, thereby improving the capacity, stability, and stiffness of the H-section steel member. In addition, the steel tube buckled outwards at the mid-height of of the H-CFRST columns, and its torsion decreased rapidly owing to the shrinking internal steel tube and peeling of the concrete in the corner. This resulted in the ‘pinching’ of the torque with respect to the torsional angle.

The torque versus torsional angle hysteresis loops of the H-CFST columns under combined compression and cyclic torsional load are shown in Fig. 9: (1) the loop of the H-CFCST column (CH1-CT1) with the high aspect ratio (L/i $\geqslant$ 17.3) and low compression ratio ($N/N_u \leqslant 0.2$) exhibits a dumpy shape. According to *Euler's stability theory* in [21], the lateral displacement of the H-CFCST column under compression increases with the aspect ratio, which is equivalent to the effect of applying an eccentric compression load to the columns at mid-height. The loops of the H-CFST columns (CH2-CT1, CH2-CT2, and RH-CT2) with low aspect ratios (L/i $\leqslant$ 12.6 or 11.9) and medium compression ratios ($N/N_u \leqslant 0.48$ for CH2-CT1 and CH2-CT2 or $N/N_u \leqslant 0.4$ for RH-CT2) have plump shapes. Thus, the compression and torsion resistance improves with increasing supporting 'effective length' of the members. (2) The unloading and reverse loading stiffness values are similar to the initial elastic stiffness; their degradation is small, which indicates that the torsional stiffness of the H-CFST columns have been hardly affected by the medium compression ratios. (3) The torsional ductility of the H-CFST columns under compression–torsion load is lower than the values under pure torsion. This is because the shear strain or conservation of shear strain energy produced by torsion decreases with increasing normal strain or conservation of normal strain energy under the compression load according to the 'energy method' which tells the work of the loads equal to the shear and normal strain energy.

3.3 Skeleton curves of torque–torsional angle procedure

The torque–torsional angle skeleton curves of the H-CFST columns are shown in Fig. 10, and the key mechanical properties are summarised in Table 3. The yielding point and yield torsional angle (θ_y) were defined by the graphical method [5], and the ultimate torsional angle (θ_u) is defined as the torsional angle at 85% peak torque or torsional angle at failure. Moreover, the ductility coefficient of the column (α_d) is expressed as the ratio between the ultimate and yield torsional angles [22].

As shown in Fig. 10, three stages (elastic, plastic, and failure stages) are presented in the torque–torsional angle skeleton curves of the H-CFST columns under cyclic torsional load, while two stages (elastic and plastic stages) occurred under combined compression and cyclic torsional loads (Figs. 10(a)–(c)). The initial stiffness, peak torsion, and ductility coefficient of CH1-CT1 under compression and cyclic torsional loads were below those under cyclic torsional load. Thus, they were reduced by the compression load at a high aspect ratio (L/i $\geqslant$ 17.3). However, the peak torsion values of CH2-CT1 and CH2-CT2 increased by 22%, while the ductility coefficient of CH2-CT2 decreased by 12.2% under compression and cyclic torsional loads compared to those under pure cyclic torsional loads. Thus, the torsional capacity of the H-CFCST column can be enhanced, whereas its ductility degenerates under compression loads for a low aspect ratio (L/i ⩽ 12.6). Compared to those under pure cyclic torsion, the peak torsion and ductility coefficient of RH-CT2 with a low aspect ratio (L/i = 11.9) decreased under static compression and cyclic torsional loads. This is believed to be because the rectangular tubes are less constrained to the concrete at the corners.

3.4 Degradation of torsional stiffness

According to [23], the secant torsional stiffness (K_θ) of H-CFST columns can be defined by the relationship between the torsional angle (θ_i) and maximal torsion (T_i):

$$K_\theta = \frac{|+T_i| + |-T_i|}{|+\theta_i| + |-\theta_i|} \quad (1)$$

The degradation of the torsional stiffness of the H-CFST columns is presented in Fig. 11. The ratio of $K_\theta/K_{\theta e}$ ($K_{\theta e}$ is the elastic torsional stiffness) decreased sharply when θ/θ_y increased ($\theta/\theta_y \leqslant 4$); however, the change in $K_\theta/K_{\theta e}$ was less pronounced than for $\theta/\theta_y > 4$. This is because the shear deformation capacity of the concrete was low, and the degradation of the torsional stiffness was accelerated by the early shear deformation failure of the concrete. In general, the applied compression has more significant effects on the torsional stiffness of H-CFCST columns with high aspect ratios (L/i = 17.3) and H-CFRST columns.

3.5 Dissipated energy

The equivalent viscous damping coefficient (h_e) was used to represent the energy dissipation capacity of the H-CFST columns; the calculation method was based on [23].

The equivalent viscous damping coefficients and energy dissipation (area of torque versus torsional angle hysteresis loops) of the H-CFST columns are shown in Figs. 12 and 13, respectively. They increased with increasing θ/θ_y in the early period ($\theta/\theta_y \leqslant 4$); over 4, the increase slowed down or even transformed into a decrease (Fig. 12(c)). In addition, the maxima of the equivalent viscous damping coefficient and energy dissipation decreased with increasing compression loads.

4. Proposed design method

The design method for the determination of the torsional capacities of the H-CFST columns based on the shear capacities of the concrete and steel components is presented in the following sections.

4.1 Shear capacity of concrete

The Mohr's circle-plane stress of the concrete element subjected to pure shear stress or combined normal and shear stresses is shown in Fig. 14. According to Fig. 14(a), the shear stress τ_c of the concrete element is equal to the maximal normal stress σ_{max}; in Fig. 14(b), the relationship between the shear strength τ_c and maximal shear stress τ_{max} is expressed as the equation $\tau_{max} = \sqrt{(\frac{-\sigma_{le}}{2})^2 + \tau_c^2}$.

The tension and compression properties are different in brittle materials like concrete, and the principle stress coordinate (σ_1,σ_2) of the concrete element is presented according to the *Mohr–Coulomb failure criterion* [21]. When the concrete is subjected to the bi-axial stresses σ_1 and σ_2 (σ_1 is tension stress and σ_2 is compression stress), the following expression holds:

$$\frac{\sigma_1}{(\sigma_{ult})_t} - \frac{\sigma_2}{(\sigma_{ult})_c} = 1. \tag{2}$$

The tensile strength of the concrete can be expressed as $f_t = (\sigma_{ult})_t = 0.26\ (f_{cu})^{2/3}$ [24-25] and its compressive strength as $f_{cu} = (\sigma_{ult})_c$. In addition, $\sigma_1 = -\frac{\sigma_{le}}{2} + \sqrt{(-\frac{\sigma_{le}}{2})^2 + \tau_c^2}$ and $\sigma_2 = -\frac{\sigma_{le}}{2} - \sqrt{(-\frac{\sigma_{le}}{2})^2 + \tau_c^2}$ are presented in Fig. 14. This leads to the following equation:

$$\frac{-\frac{\sigma_{le}}{2} + \sqrt{(-\frac{\sigma_{le}}{2})^2 + \tau_c^2}}{(0.26 f_{cu}^{2/3})} - \frac{-\frac{\sigma_{le}}{2} - \sqrt{(-\frac{\sigma_{le}}{2})^2 + \tau_c^2}}{f_{cu}} = 1. \tag{3}$$

The normal stress σ_{le} is produced by the axial force, which is f_{cu} caused by the cube compression test. The τ_c in Eq. (3) can be solved with the iterative method. The relationship of τ_c and σ_{le} of the concrete (f_{cu} = 40.7 MPa) under shear and normal stresses is presented in Table 4.

According to Table 4, (1) the maximal shear stress τ_c of the concrete is 5.59 MPa when its normal stress σ_{le} reaches 20.3 MPa; 2) the shear stress τ_c of the concrete is zero when its normal stress σ_{le} increases to 40.7 MPa (f_{cu}); thus, its compression strength increases to the maximum, whereas the shear strength decreases to zero; 3) owing to the radial constraint of the steel tube, the normal stress σ_{le} of the concrete remains f_{cu} until the force acting on the steel tube exceeds the compression and shear strength.

4.2 Shear capacity of steel

Mohr's circle-plane stress of the steel element subjected to shear stress or combined normal and shear stresses is shown in Fig. 15. According to Fig. 15(a), the shear stress τ_{si} of the steel element is equal to the maximal shear stress τ_{max}, and according to Fig. 15(b), the relationship between the shear stress τ_{si} and maximal shear stress τ_{max} can be expressed as $\tau_{\max} = \sqrt{(\frac{-\sigma_{le}}{2})^2 + \tau_{si}^2}$, where σ_{le} is the normal stress produced by the compression.

To determine the shear strength τ_s of the steel under different normal stress values, the failure criterion of the *maximum distortion energy theory* developed by Huber and von Mises [18] was considered. The maximal distortion of a regular hexahedron subjected to the principal normal stress is presented in [21]. Based on the equations of the strain energy density u $=(1/2)\sigma\varepsilon$ and u $= (1/2)(\sigma_1\varepsilon_1+\sigma_2\varepsilon_2+\sigma_3\varepsilon_3)$, Eq. (4) is presented as follows:

$$u = \frac{1}{2E}\left[\sigma_1^2 + \sigma_2^2 + \sigma_3^2 - 2\nu(\sigma_1\sigma_2 + \sigma_1\sigma_3 + \sigma_2\sigma_3)\right]. \tag{4}$$

When $\sigma_1,\sigma_2,\sigma_3$ are substituted into Eq. (5), the strain energy density u_d can be obtained:

$$\sigma_1^{'} = \sigma_1 - \sigma_{avg}, \sigma_2^{'} = \sigma_2 - \sigma_{avg}, \sigma_3^{'} = \sigma_3 - \sigma_{avg}, \sigma_{avg} = \frac{\sigma_1 + \sigma_2 + \sigma_3}{3}, \tag{5}$$

$$u_d = \frac{1}{6E}(1+\nu)((\sigma_1^{'} - \sigma_2^{'})^2 + (\sigma_2^{'} - \sigma_3^{'})^2 + (\sigma_3^{'} - \sigma_1^{'})^2). \tag{6}$$

Under uniaxial tension, $\sigma_1^{'} = \sigma_Y$, $\sigma_2^{'} = \sigma_3^{'} = 0$, $(u_d)_Y = \frac{1+\nu}{3E}\sigma_Y^2$. Consequently,

$$(\sigma_1^{'} - \sigma_2^{'})^2 + (\sigma_2^{'} - \sigma_1^{'})^2 + (\sigma_3^{'} - \sigma_1^{'})^2 = 2\sigma_Y^2. \tag{7}$$

Under plane stress, $\sigma_3^{'} = 0$, and Eq. (6) can be shortened as follows:

$$u_d = \frac{1+\nu}{3E}(\sigma_1^{'2} - \sigma_1^{'}\sigma_2^{'} + \sigma_2^{'2}). \tag{8}$$

As the maximum distortion energy theory requires, $u_d = (u_d)_Y$ and $(u_d)_Y = \frac{1+\nu}{3E}\sigma_Y^2$. In the case of biaxial stress, the following equation holds:

$$\sigma_1'^2 - \sigma_1'\sigma_2' + \sigma_2'^2 = \sigma_Y{}^2 . \tag{9}$$

In the case of a pure torsion test, $\sigma_1 = \sigma_1' = \tau_{si}$, $\sigma_2 = \sigma_2' = -\tau_{si}$, which leads to Eq. (10):

$$\tau_{si} = \sigma_1 = \sigma_1' = \frac{\sigma_Y'}{\sqrt{3}} = \frac{f_y}{\sqrt{3}} . \tag{10}$$

Because

$$\sigma_{avg} = -\frac{\sigma_{le}}{2}, \sigma_1 - \sigma_{avg} = \sqrt{(\frac{\sigma_{le}}{2})^2 + \tau_{si}^2}, \sigma_2 - \sigma_{avg} = -\sqrt{(\frac{\sigma_{le}}{2})^2 + \tau_{si}^2},$$

Eqs. (5) and (7) can be used to establish Eq. (11):

$$[(\frac{\sigma_{le}}{2})^2 + \tau_{si}^2] + [(\frac{\sigma_{le}}{2})^2 + \tau_{si}^2] + [(\frac{\sigma_{le}}{2})^2 + \tau_{si}^2] = \sigma_Y{}^2 = f_y{}^2 , \tag{11}$$

which can be converted into

$$\tau_{si} = \sqrt{\frac{f_y{}^2}{3} - \frac{1}{4}\sigma_{le}^2} \ (0 \leqslant \sigma_{le} \leqslant \frac{2}{\sqrt{3}} f_y). \tag{12}$$

Eq. (12) states that the normal stress of a steel tube and welded H-section steel σ_{le} is up to ($2 f_y / \sqrt{3}$) when its shear strength τ_{si} becomes zero. The steel tubes did not crack or experience failure in the experiments, in particular in the compressive torsional tests of the H-CFST columns. Thus, it is appropriate to replace f_y in Eq. (12) with the yielding tensile strength of steel.

4.3 Torsional capacity of H-CFST columns

The shear and normal stresses of the H-CFST columns subjected to compression–torsion load in the failure state are shown in Fig. 16; the concrete is divided into two zones: an elastic core and a plastic annulus. The shear stress of the concrete plastic annulus is denoted as τ_c, while the shear stresses of the H-section steel and steel tube are represented by τ_{s1} and τ_{s2}, respectively. Because of the in-filled concrete, the shear stress transmission of the flanges of the welded H-section steel was considered a closed loop. The normal stress values of the steel and concrete (σ_{le}) affect their shear capacity.

4.3.1 Torsional capacity of H-CFCST columns

The shear and normal stresses of the H-CFCST columns subjected to compression–torsion load and in the failure state are shown in Fig. 16(a), and the shear stress distribution of the cross-section is shown in Fig. 17(a). The torsional capacity of the cylinder concrete is defined as T_{cu}, which includes the torsional capacities of the plastic annulus T_{pa} and elastic core cylinder T_{ec}. The radius of the internal cylinder concrete is ρ, and the maximal radius of the elastic core and plastic annulus are denoted as c_1 and c_2, respectively. Moreover, the maximal shear stress of the elastic core is τ_{c}. According to the proportionality of triangles and Hooke's law, the shear stress of the elastic core concrete τ can be expressed as $(\rho/c)\,\tau_{\mathrm{c}}$ for the cross-section of the H-CFCST column, and the shear stresses of the H-section steel member and steel tube can be denoted as τ_{s1} and τ_{s2}, respectively.

Specifically, each area element dA of the concrete that is located at ρ is subjected to a force $dF = \tau\, dA$. The torsion produced by this force is $dT = \rho\,(\tau\, dA)$, and the torsional capacity of the entire cross-section of the concrete cylinder is as follows:

$$T_{cu}=T_{pa}+T_{ec}=\int_{c_1}^{c_2}\rho\tau_{\mathrm{c}}2\pi\rho d\rho+\int_{0}^{c_1}\rho\left(\frac{\rho}{c_1}\tau_c\right)2\pi\rho d\rho=\frac{2\pi\tau_{\mathrm{c}}(c_2^{\,3}-c_1^{\,3})}{3}+\frac{\pi\tau_c c_1^{\,3}}{2}. \tag{13}$$

Similarly, each area element $t_{Cs}\,ds$ of the circular steel that is located at c_2 is subjected to a force $dF = \tau_{\mathrm{s2}}\, dA = \tau_{\mathrm{s2}}\, t_{Cs}\, ds$. The torsion produced by this force is $dT = c_2\,(\tau_{\mathrm{s2}}\, t_{Cs}\, ds) = 2\tau_{\mathrm{s2}}\, t_{Cs}\, dA$, and the torsion of the flange of the H-section steel is similar to that of the circular steel, which can be expressed as $2\tau_{\mathrm{s1}}\, t_{Hs,f}\, A_{s1}$. The torsion of the web of the H-section steel can be determined with the torsional capacity equation ($\tau_{\mathrm{s1}}J/0.5L_{Hs,w}$). Therefore, the torsional capacity of the circular steel tube and H-section steel member of the H-CFCST column can be calculated with Eq. (14):

$$T_{su}=T_{Cs}+T_{Hs}=\int_0^{L_m}c_2\tau_{s2}t_{Cs}ds+\left(2\tau_{s1}t_{Hs,f}A_{s1}+\frac{2\tau_{s1}J}{L_{Hs,w}}\right)=2\tau_{s2}t_{Cs}A_{Cs}+2\tau_{s1}t_{Hs,f}A_{s1}+\frac{2\tau_{s1}J}{L_{Hs,w}}. \tag{14}$$

Accordingly, the torsional capacity of the H-CFCST column can be determined as follows:

$$T_u=T_{cu}+T_{su}=\frac{2\pi\tau_{\mathrm{c}}(c_2^{\,3}-c_1^{\,3})}{3}+\frac{\pi\tau_c c_1^{\,3}}{2}+2\tau_{s2}t_{Cs}A_{Cs}+2\tau_{s1}t_{Hs,f}A_{s1}+\frac{2\tau_{s1}J}{L_{Hs,w}}. \tag{15}$$

4.3.2 Torsional capacity of H-CFRST columns

The shear and normal stresses of the H-CFCST columns subjected to compression–torsion loads and in the failure state are shown in Fig. 16(a), and the shear stress of the cross-section subjected to torsion or combined compression and torsion is shown in Fig. 17(b). The torsional capacity of the rectangular concrete is defined as T_{cu}; it consists of the torsional capacity of the plastic annulus T_{pa} and elastic core of the cylinder T_{ec}. The side length of any element of the internal rectangular concrete is x, and the maximal side length of the elastic core and plastic annulus of the cylinder concrete are b_1 and b_2, respectively. Moreover, an unbalance coefficient α should be added to τ_c because the distribution of the shear stress in the cross-section is inhomogeneous. The value of the unbalance concrete coefficient α is 0.5, which is the average shear value coefficient of the middle and corner point of the rectangular side. According to the proportionality of triangles and Hooke's law ($\tau = G\gamma$) and [$\gamma = (\rho/b)\ \gamma_{max}$], the shear stress of the elastic core can be expressed as [$\tau = (x/b_1)\ \ \alpha\ \tau_c$] for the H-CFRST column.

Specifically, each area element dA of the concrete that is located at x is subjected to a force $dF = \tau\ dA$. The torsion produced by this force is $dT = (x/2)(\tau\, dA)$. Because the shear stress of the plastic annulus and elastic core are τ_c and $\tau = (x/b_1)\ \alpha\ \tau_c$, dT_{pa} and dT_{ec} can be expressed as $(x/2)\ \alpha\ \tau_c\ 4xdx$ and $(x/2)\ [(x/b_1)\ \alpha\ \tau_c\ 4xdx]$. The torsional capacity of the entire cross-section of the cylinder concrete can be obtained with Eq. (16):

$$T_{cu}=T_{pa}+T_{ec}=\int_{b_1}^{b_2}\frac{x}{2}(\alpha\tau_c)4xdx+\int_0^{b_1}\frac{x}{2}(\frac{x}{b_1}\alpha\tau_c)4xdx=\frac{2}{3}\alpha\tau_c(b_2^3-b_1^3)+\frac{1}{2}\alpha\tau_c b_1^3. \quad (16)$$

The derivation process of the torsional capacity T_{su} of the rectangular steel tube and H-section steel is similar to that of Eq. (17):

$$T_{su}=T_{Rs}+T_{Hs}=\int_0^{L_m}c_2\tau_{s2}t_{Rs}ds+2\tau_{s1}t_{Hs,f}A_{s1}+\frac{2\tau_{s1}J}{L_{Hs,w}}=2\tau_{s2}t_{Rs}A_{Rs}+2\tau_{s1}t_{Hs,f}A_{s1}+\frac{2\tau_{s1}J}{L_{Hs,w}}. \quad (17)$$

Thus, the torsional capacity of the H-CFRST column can be determined as follows:

$$T_u=T_{su}+T_{cu}=\frac{2}{3}\alpha\tau_c(b_2^3-b_1^3)+\frac{1}{2}\alpha\tau_c b_1^3+2\tau_{s2}t_{Rs}A_{Rs}+2\tau_{s1}t_{Hs,f}A_{s1}+\frac{2\tau_{s1}J}{L_{Hs,w}}. \quad (18)$$

4.4 Discussion: equation for shear capacity of steel

The shear strength τ_{si} of the steel in Eq. (12) is based on Mohr's circle-plane stress and the von

Mises failure criterion. Bresler and Pister [26] determined the shear strength of the concrete of a thin-walled cylinder by torsion tests. According to the results, the shear stress strength of steel in CFSTs is easier to determine with torsion tests than that of hollow thin-walled steel tubes, in particular when the steel experiences combine normal stress and shear stress. The torsional capacity data of the CFST columns under pure cyclic and compressive torsion in [5] [9] [27] [28] are summarised in Table 5. According to Eq. (15) in Section 4.3 and the theoretical analysis, the tested shear stress strength τ_{si} of the steel of the CFST columns under normal stress can be expressed with Eq. (19):

$$\tau_{si} = (T_u - \frac{\pi \tau_c c_2^3}{2}) / (2 t_{Cs} A_{Cs}) . \tag{19}$$

The torsional capacity T_u in Eq. (19) was replaced by the experiment results in [5] [9] [27] [28] and τ_c by the calculated results of Eq. (3), and the tested shear strength τ_{si} or τ_{si}/f_u of the steel under different normal stresses σ_{le} or σ_{le}/f_u are listed in Table 5. Evidently, the theoretical value of τ_{si}/f_u is lower than -3.8% to 15.5% of the tested value when the normal stress ratio σ_{le}/f_u is not over 0.24. Thus, the theory of the shear stress strength based on the von Mise failure criterion is accurate when the steel tube experiences moderate normal stress.

5. Comparison of results

The torsional capacities of the H-CFST columns under monotonic compression and cyclic torsion were determined by the proposed design method in Section 4, and the predicted results were compared with the test results (Fig. 18). The proposed design method provides conservative results for most specimens, and the mean predicted-to-tested ratio is 0.89 with a coefficient of variation of 0.15. In general, the results show that the capacity of the H-CFST columns under monotonic compression and cyclic torsion can be predicted accurately and consistently with the design method. The theoretical contribution of the H-section steel members, steel tubes, and concrete to the torsional capacity of the H-CFST columns are presented in Fig. 19. Owing to its high shear strength and long level arm, the external steel tube has the greatest contribution among the three components.

6. Conclusions

This is the first study to investigate the seismic performance of this new type of H-CFST columns under cyclic torsional and compression–cyclic torsional loads experimentally and thereafter proposed the design methods. Based on the attempt to analyse the torsional behaviours and mechanical properties of H-CFST columns on torsion and compressive torsion, the following observations and conclusions are made:

(1) The torsional behaviour of H-CFST columns under torsion or compression and torsion is revealed from the tests which is carried out by the designed newly setup.

(2) The shear capacities of the steel and concrete under normal stress or combined normal and shear stress are firstly deduced by the Mohr's circle-plane stress, *Mohr–Coulomb failure criterion* and *maximum distortion energy theory*, and a comparison of results using the shear capacity of steel shows good agreement with test results.

(3) The design method for the determination of the torsional capacity of H-CFST columns under torsion or compression and torsion is proposed based on the test results.

Acknowledgements

The authors are grateful to the financial support provided by Fok Ying Tung Education Foundation, Chongqing Science and Technology Bureau (cstc2019jcyj-zdxm0088), 111Project (B18062) and Fundamental Research Funds for the Central Universities (2019CDQYTM028).

Notation

b_1	width and height of welded H-section steel
b_2	width and height of steel tube
c_1	maximal radius of elastic core
c_2	maximal radius of plastic annulus
f_{cu}	compression strength of concrete
f_t	axial tension strength of concrete
f_y	tension strength of steel
h_e	equivalent viscous damping coefficient
i	radius of gyration; equal to radius of circular column divided by 0.707 and equal to the side length o rectangular column divided by 0.401
n	ratio of axial force load and compressive bearing capacity
t_{Cs}	thickness of circular steel tube
t_{Hs}	thickness of web of welded H-section steel
$t_{Hs,f}$	thickness of flange of welded H-section steel
t_{Rs}	thickness of rectangular steel tube
x	side length of elastic core and plastic annulus; from 0 to b_2
A_{Cs}	cross-sectional area of H-CFCST column
A_{Rs}	cross-sectional area of H-CFRST column
A_{s1}	area of elastic core of H-CFST column
G	shear modulus of steel

J polar moment of inertia of web of welded H-section steel

K_{θ} torsional secant stiffness

$K_{\theta e}$ torsional yield stiffness

L height of specimen

$L_{\mathrm{Hs,w}}$ length of web of welded H-section steel

N applied axial force load

N_u tested compressive bearing capacity

$N_{\mathrm{u,c}}$ theoretical compressive bearing capacity

S area of hysteresis loop

T_i maximal torsion of class i cycle

T_{cu} yielding torsional moment capacity of cylinder concrete

T_{ec} torsional moment capacity due to elastic core of cylinder concrete

T_{pa} torsional moment capacity due to plastic annulus of cylinder

$T_{u0,t}$ torsional capacity under torsion

$T_{u0,t}$ measured torsional capacity under torsion

$T_{u0,c}$ calculated torsional capacity under torsion

$T_{uc,t}$ measured torsional capacity under compression and torsion

$T_{uc,c}$ calculated torsional capacity under compression and torsion concrete

T_{su} torsional capacity of steel tube and welded H-section steel

T_{u} torsional capacity of H-CFST columns

T_{Cs} yield torsional moment capacity of steel tube

T_{Hs} yield torsional moment capacity of welded H-section steel

$\Delta\theta$ increment in torsional angle

θ torsio□al angle

θ_i maximal torsional angle of class i cycle

θ_u ultimate torsional angle

θ_y yield torsional angle

τ_{c} failure shear stress of concrete under pure shear or shear and compression

τ_{s1} failure shear stress of welded H-section steel under pure shear or shear and compression

τ_{s2} failure shear stress of steel tube under pure shear or shear and compression

α_d ductility coefficient of column

α unbalance concrete coefficient of shear stress

ρ radius of elastic core and plastic annulus; from 0 to c_2

σ_{le} normal stress of steel tube of H-CFST column

$\sigma_{\mathrm{le,c}}$ normal stress of concrete of H-CFST column

σ_{avg} average principal stress

σ_1 principal normal stress of x' -axial direction

σ_2 principal normal stress of y' -axial direction

σ_3 principal normal stress of z' -axial direction

σ_1', σ_2', σ_3' remaining part of principle normal stress of σ_1-σ_{avg}, σ_2-σ_{avg}, σ_3-σ_{avg} causes distortio

γ shear strain

REFERENCES

[1] Suriya Prakash， Abdeldjelil Belarbi， Young-Min You. Seismic performance of circular RC columns subjected to axial force, bending, and torsion with low and moderate shear. Eng. Struct, Vol. 32(1), 2010: 46-59.

[2] Wenjing Wang, Hua Ma, Zhenbao Li, Zhenyun Tang. Size effect in circular concrete filled steel tubes with different diameter-to-thickness ratios under compression. Engineering Structures, Vol.

151(15), 2017:554-567.

[3] Lin-hai Han. Concrete-filled Steel Tubular Structures—Theory and Practice，Beijing: Science Press, 2007: 1-739.

[4] Mohamed Elchalakani, X.L. Zhao, Concrete-filled cold-formed circular steel tubes subjected to variable amplitude cyclic pure bending, Eng. Struct, Vol. 30(2), 2008: 287–299.

[5] Yu-hang Wang. Study on torsion effect in concrete filled steel tube piers of curved girder bridge [Ph.D. thesis]. Beijing: Tsinghua University，2013: 1-139.

[6] Yu-hang Wang，Jian-guo Nie，Jian-sheng Fan. Cross section shear strain distribution of rectangular concrete filled steel tube columns subjected to torsion. Beijing：Engineering Mechanics journal， Vol. 31(5)，2014: 101-119.

[7] Yu-hang Wang，Jian-guo Nie，Jian-sheng Fan. Study on the torsion behaviour of concrete filled steel tube column with circular section. Beijing：Engineering Mechanics journal，Vol. 31(3), 2014: 222-227.

[8] Jian-guo Nie，Yu-hang Wang，Jian-sheng Fan. Experimental study on seismic behaviour of concrete filled steel tube columns under torsion and compression–torsion cyclic load. Journal of Constructional Steel Research, Vol. 79, 2012: 115-126.

[9] Beck J, Kiyomiya O．Fundamental pure torsional properties of concrete filled circular steel tubes. Materials, Conc. Struct. Pavaments, JSCE, 2003, 60(739):285-296.

[10] Shuai Li， Lin-Hai Han，Chao Hou. Concrete-encased CFST columns under combined compression and torsion: Analytical behaviour. Journal of Constructional Steel Research, Vol. 144, 2018: 236-252.

[11] Fa-xing Ding, Tao Zhang, Xue-mei Liu, Zhao-Hui Lua, Qiang Guo, Guo-shuai Jiang. Behaviour of steel-reinforced concrete-filled square steel tubular stub columns under axial loading. Thin-Walled Structures, Vol. 119, 2017: 737–748.

[12] M. Elchalakani, X.L. Zhao, R. Grzebieta. Tests on concrete filled double-skin (CHS outer and SHS inner) composite short columns under compression. Thin-Walled Struct., Vol. 40, 2002: 415-441.

[13] Yu-Hang Wang, Guo-Bing Lu, Xu-Hong Zhou. Experimental study of the cyclic behaviour of concrete-filled double skin steel tube columns subjected to torsion. Thin-Walled Structures, Vol. 122, 2018: 425-438.

[14] Mohamed Elchalakani, M.F. Hassanein, Ali Karrech, Sabrina Fawzia, BoYang, V.I.Patel. Experimental tests and design of rubberised concrete-filled double skin circular tubular short columns. Structures, Vol. 15, 2018:196-210.

[15] Mojtaba Farahi, Amin Heidarpour, Xiao-Ling Zhao, Riadh Al-Mahaidi. Compressive behaviour of concrete-filled double-skin sections consisting of corrugated plates, Eng. Struct, Vol. 111, 2016: 467–477.

[16] Talha Ekmekyapar, Hussein Ghanim Hasan. The influence of the inner steel tube on the compression behaviour of the concrete filled double skin steel tube (CFDST) columns. Marine Structures, Vol.66, 2019: 197-212.

[17]·Hussein Ghanim Hasan, Talha Ekmekyapar. Mechanical Performance of Stiffened Concrete Filled Double Skin Steel Tubular Stub Columns under Axial Compression. KSCE Journal of Civil Engineering, Vol.23(5), 2019: 2281-2292.

[18] Hong Huang, Mengcheng Chen, Binjie Huang. Experimental study of concrete-filled double-skin circular steel tube subject to pure torsion. China HeiFei: Journal of Experimental Mechanics, Vol.27, Jun.2012:288-294. (In Chinese)

[19] Hong Huang, Mengcheng Chen, Binjie Huang. Experimental study of concrete-filled double-skin circular steel tube subject to compression and torsion. HeiFei: Journal of Experimental Mechanics, Vol.30, Feb.2015. (In Chinese)

[20] Yan-li Shi. Research on shear behaviour of concrete filled steel tubular members with internal profiled steel [Ph.D. thesis]. Lanzhou: Lanzhou University, 2018:1-156.

[21] R. C. Hibbeler. Mechanics of Materials, Beijing: Higher Education Press, 2013:177-673.

[22] GB 50152-92 Standard Methods for Testing of Concrete Structures. China Architecture & Building Press (1992).

[23] Yu-Hang Wang, Wei Wang, Ju Chen. Seismic behavior of steel tube confined RC columns under compression-bending-torsion combined load. Journal of Constructional Steel Research, Volume 143, April 2018: 83-96.

[24] Chuan-zhi Wang, Zhi-ming Teng. The theory of reinforced concrete structure, Beijing: China building industry press, 1985. (In Chinese)

[25] Zhi-ming Teng. Basic members of reinforced concrete structure, the second edition, Beijing: China building industry press, 1987. (In Chinese)

[26] Bresler B, Piser K S. Strength of concrete under combined stresses. ACI, sept 1958: 321~346.

[27] Yu-Hang Wang, Shuo-Li, Xu hong-Zhou, Jie peng-Liu. Study on mechanical behavior of concrete filled steel tubular short columns under compound bending-shear-torsion load. Beijing：Journal of building structures，Vol. 38(11), 2017: 1-12. (In Chinese)

[28] Ji-Shan Xu, George Lee, K.C.Chang, Kunitomo. Experimental studies on steel tube, cored concrete and concrete filled steel tube short column under compression and torsion. Beijing：Journal of Beijing institute of civil engineering and architecture, Vol. 2, 1991:1-10. (In Chinese)

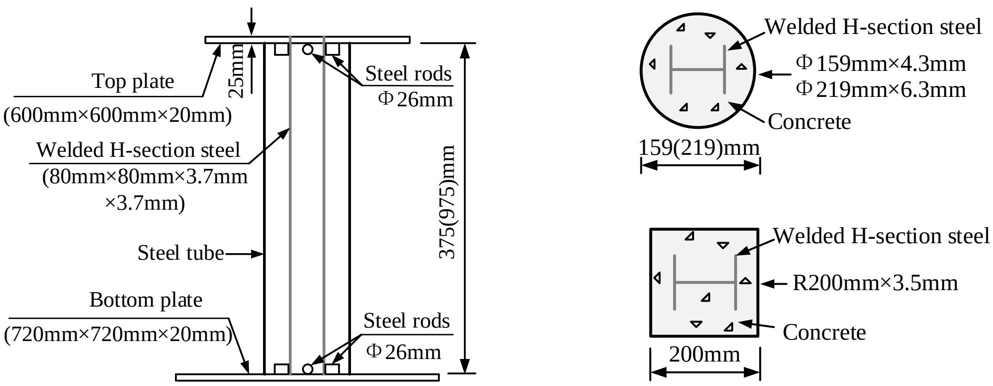

(a) Elevation view (b) Cross-section

Fig. 1 Geometric dimensions of H-CFST columns

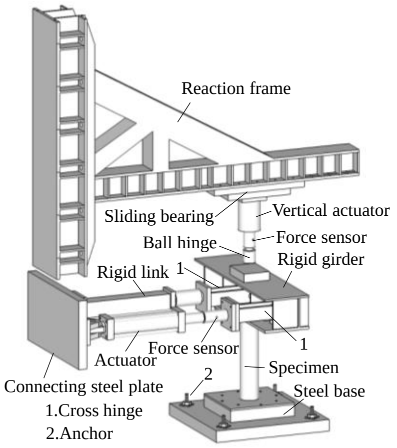

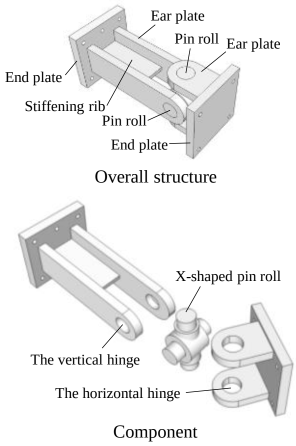

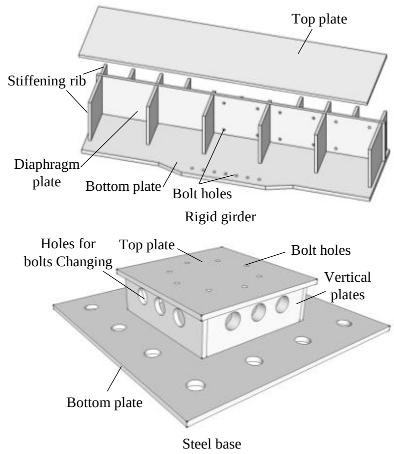

(a)Sketch of set-up (b) Sketch of cross hinge (c) Sketch of rigid girder and steel base

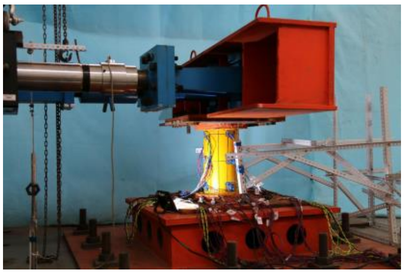

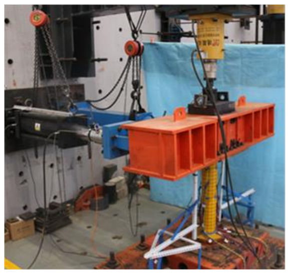

(d) Set-up of torsion experiments (e) Set-up of compression–torsion experiments

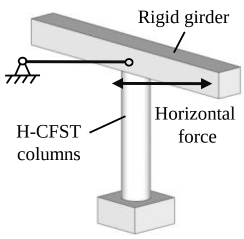

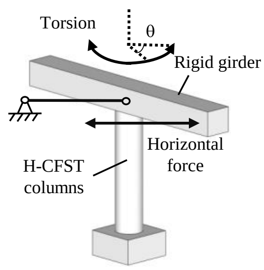

(f) Torsion (g) Compression–torsion

Fig. 2 Test set-ups for torsion and compression–torsion experiments

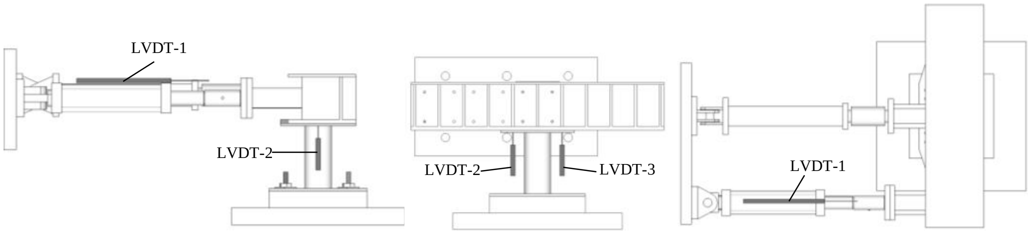

(a) Side view (b) Front view (c) Top view

Fig. 3 Measurement points of displacement gauges

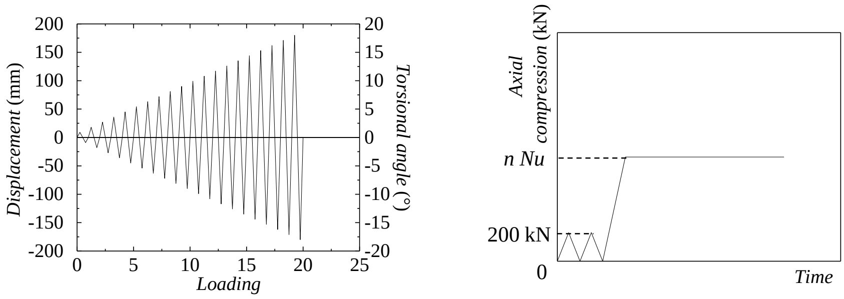

(a) Torsional loading (b) Compression

Fig. 4 Cyclic loading mode

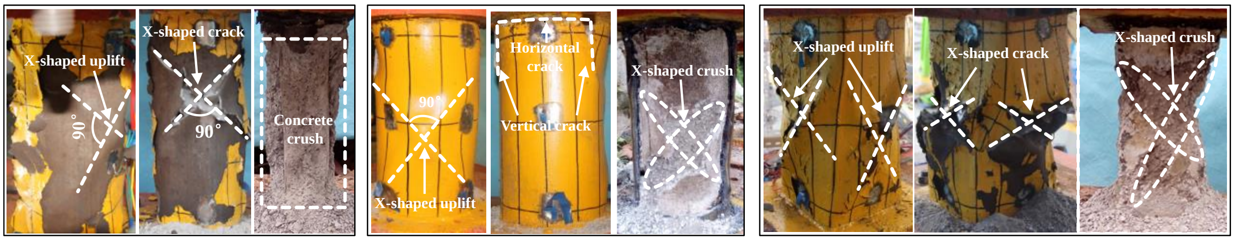

$\theta \approx 22.3°$ $\theta \approx 23.4°$ $\theta \approx 23.4°$ $\theta \approx 19.3°$ $\theta \approx 20.9°$ $\theta \approx 20.9°$ $\theta \approx 13.8°$ $\theta \approx 19.3°$ $\theta \approx 19.3°$

(a) CH1-T (b) CH2-T (c) RH-T

Fig. 5 Failure modes of H-CFST columns under torsion

$\Delta = 21.7$mm $\Delta = 8.8$mm

(a) CH2-C (b) RH-C

Fig. 6 Failure modes of H-CFST columns under compression

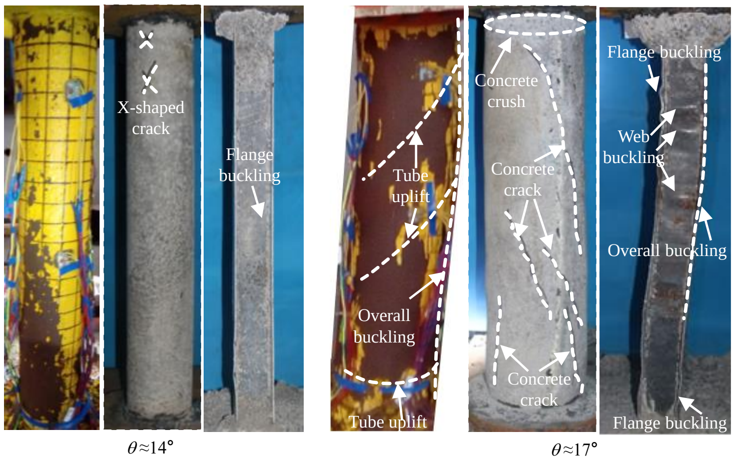

(a) CH1-CT1 (b) CH2-CT1

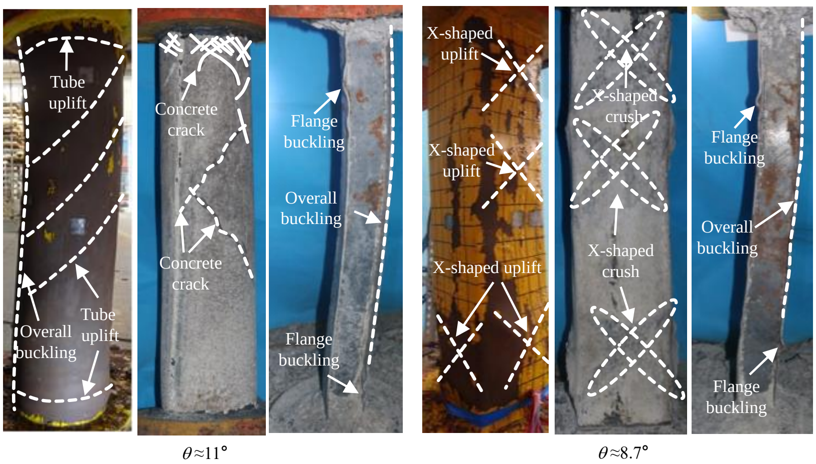

(c) CH2-CT2 (d) RH-CT2

Fig. 7 Failure modes of H-CFST columns under compression–torsion load

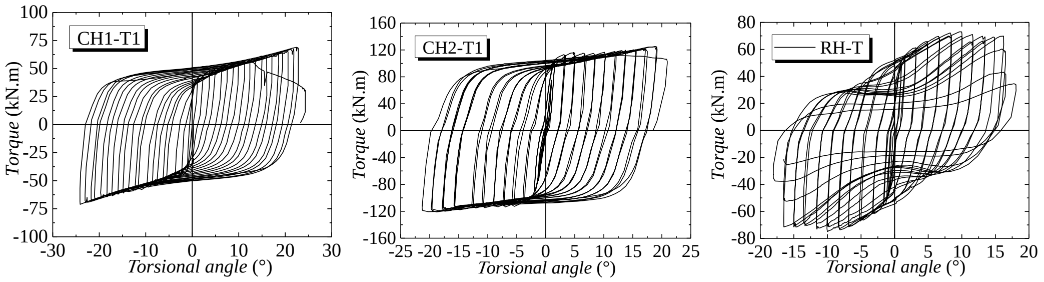

(a) (b) (c)

Fig. 8 Hysteretic torque–torsional angle curves of H-CFST columns under torsion

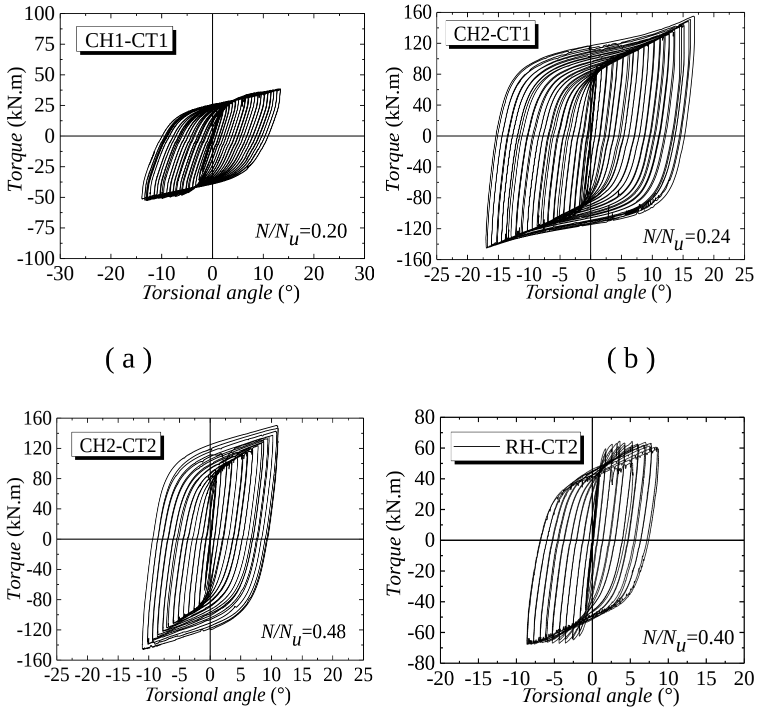

(a) (b)

(c) (d)

Fig. 9 Hysteretic torque–torsional angle curves of H-CFST columns under compression–torsion load

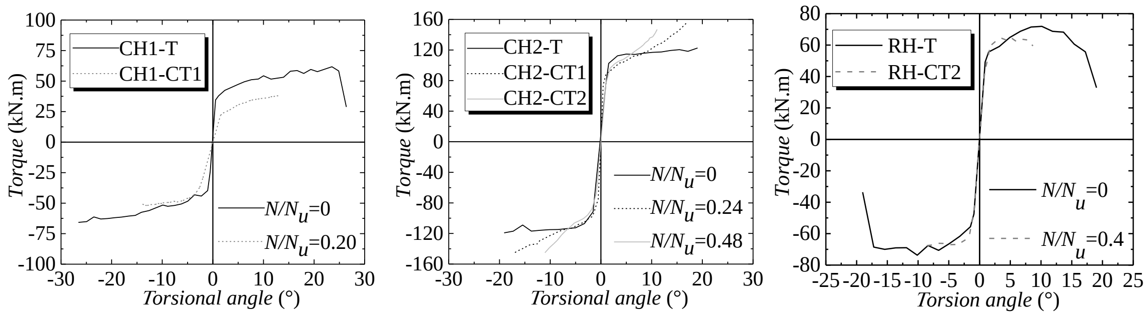

(a) (b) (c)

Fig. 10 Skeleton torque–torsional angle curves

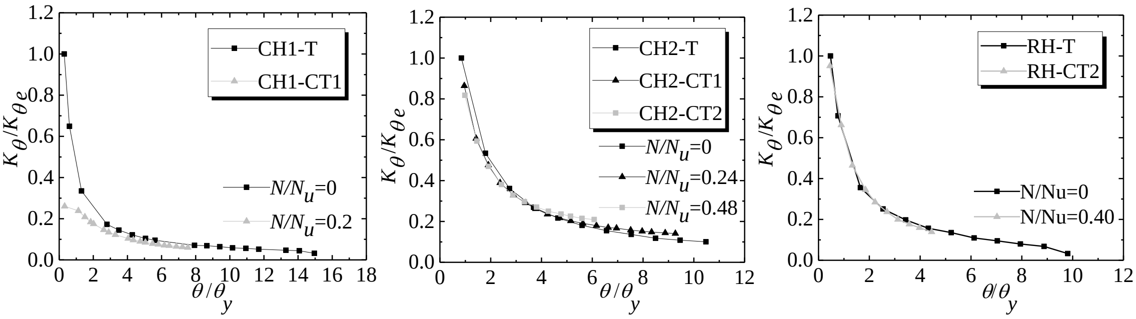

(a) (b) (c)

Fig. 11 Degradation curves of torsional stiffness

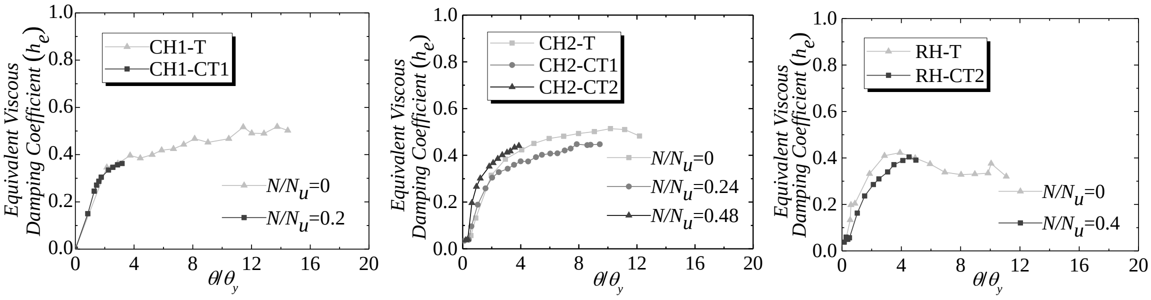

(a) (b) (c)

Fig. 12 Equivalent viscous damping coefficient of torsion

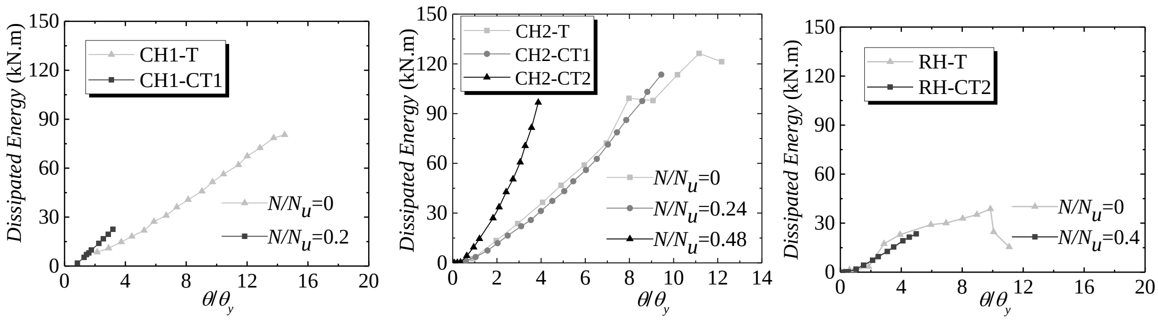

(a) (b) (c)

Fig. 13 Dissipated energy

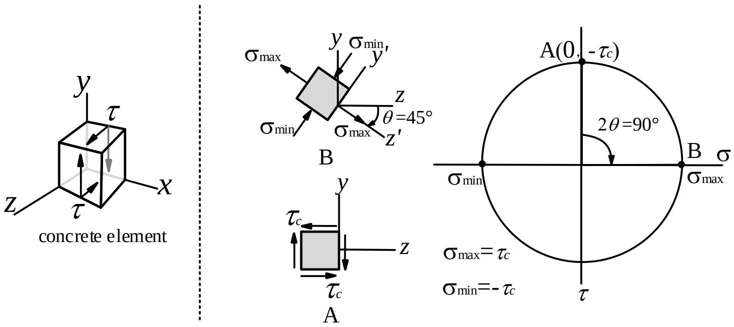

(a) Concrete element under shear stress

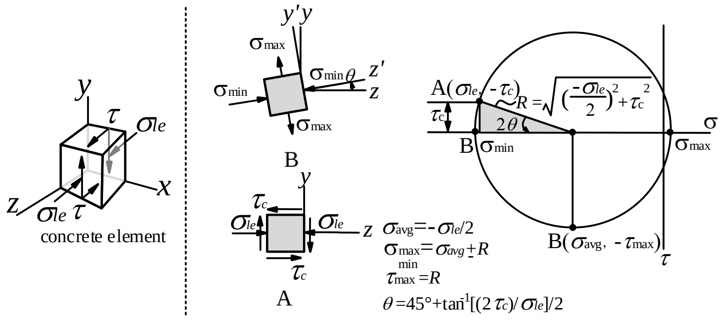

(b) Concrete element under normal and shear stresses

Fig. 14 Mohr's circle-plane stress of concrete element in H-CFST column

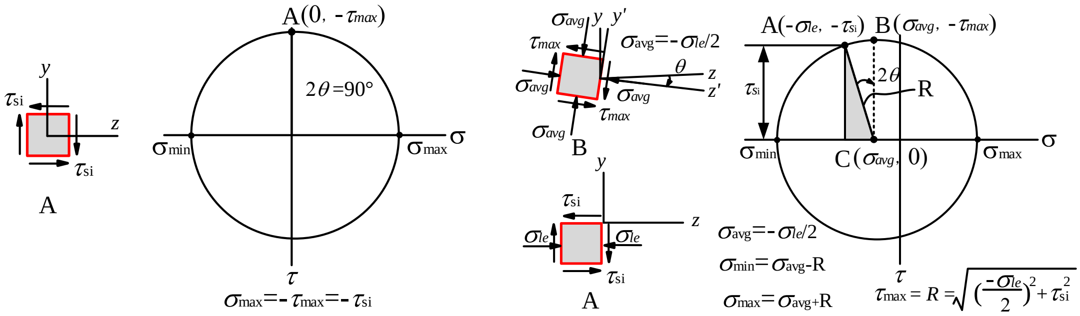

(a) Steel element under shear stress (b) Steel element under normal and shear stresses

Fig. 15 Mohr's circle-plane stress of steel element in H-CFST column

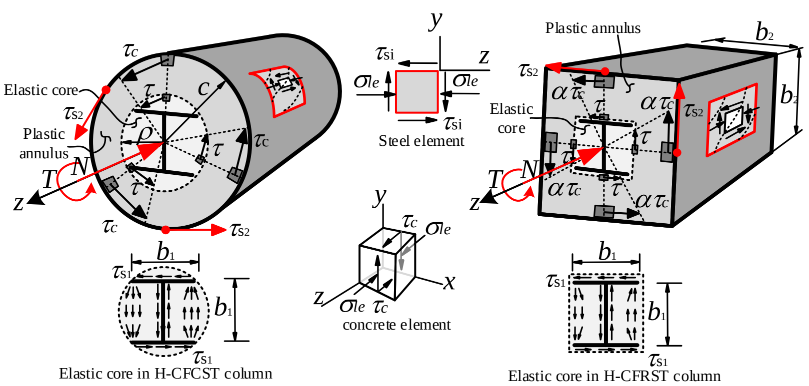

(a) H-CFCST column (b) H-CFRST column

Fig. 16 Stress distribution of H-CFST columns under compression and torsion

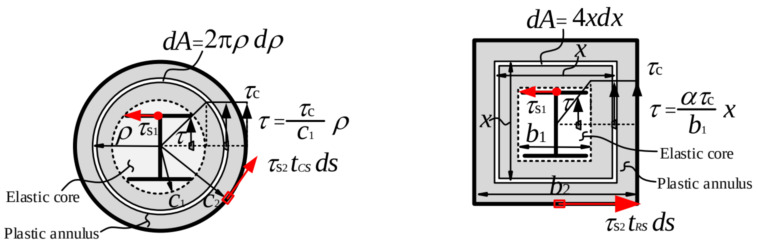

(a) H-CFCST column (b) H-CFRST column

Fig. 17 Shear stress and area element of cross-section of H-CFST columns

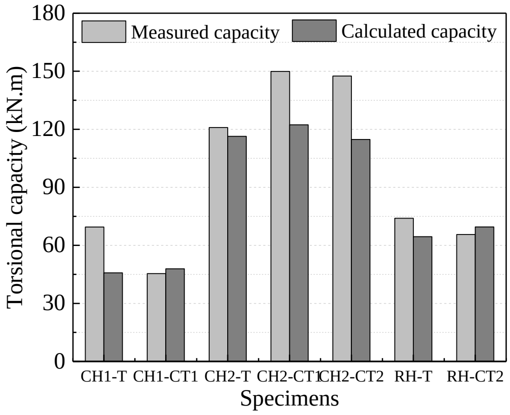

Fig. 18 Comparison of experimentally and numerically predicted torsional capacity

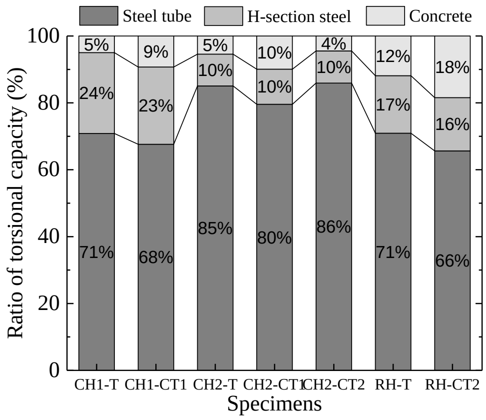

Fig. 19 Contribution of H-section steel, steel tube, and concrete to torsional capacity of H-CFST columns

Table 1: Details of H-CFST columns

H-CFST column	Details	Tube size (mm)	Height (L/mm)	L/i	Axial force (kN)	n / ($n=N/N_u$)	Loading mode
CH1-T	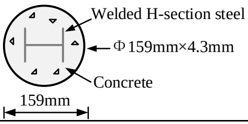	ϕ159×4.3	375	6.7	0	0	Torsion
CH1-CT1			975	17.3	396	0.2	Compression–torsion
CH2-T	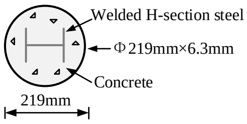	ϕ219×6.3	375	4.8	0	0	Torsion
CH2-C			975	12.6	3088	1.0	Compression
CH2-CT1			975	12.6	730	0.24	Compression–torsion
CH2-CT2			975	12.6	1459	0.48	Compression–torsion
RH-T	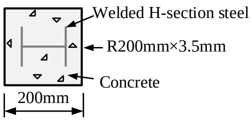	R200×3.5	375	4.6	0	0	Torsion
RH-C			975	11.9	2388	1.0	Compression
RH-CT2			975	11.9	952	0.4	Compression–torsion

Where n is the ratio of the axial force load to compressive bearing capacity, L/i the aspect ratio, L the specimen height, and i the radius of gyration

Table 2: Material properties of steel materials

Mechanical properties	Types of steel materials			
	R 200×3.5	Φ159×4.3	Φ219×6.3	Welded H-section steel
Yield strength (MPa)	283.0	329.0	361.3	353.3
Ultimate strength (MPa)	403.7	475.5	481.9	430.3
Modulus of elasticity (GPa)	220	230	210	230

Table 3 Mechanical characteristics of specimens determined in tests

Specimens	**Yield torsion (kN.m)**	**Yield torsional angle (°)**	**Peak torsion (kN.m)**	**Peak torsional angle (°)**	**Ultimate torsion (kN.m)**	**Ultimate torsional angle (°)**	**Ductility factor**
CH1-T	41.3	1.8	69.5	23.5	69.5	23.5	13.1
CH1-CT1	36.4	4.1	45.4	13.1	44.7	14.0	3.4
CH2-T	99.4	1.8	120.9	20.2	120.9	20.9	13.9
CH2-CT1	95.0	1.8	149.9	16.9	149.9	16.9	13.0
CH2-CT2	100.7	3.0	147.5	11.0	147.5	11.0	12.2
RH-T	61.4	1.9	74.0	10.0	62.9	16.5	8.7
RH-CT2	58.2	1.6	65.6	5.2	62.6	8.6	5.4

Table 4 Relationship of τ_c and σ_{le} of concrete under shear and normal stress (f_{cu} = 40.7 MPa)

σ_{le} /(MPa)	0	5.0	10.0	15.0	20.3	25.0	30.0	35.0	37.0	39.0	40.0	40.7
τ_c /(MPa)	3.26	4.35	5.12	5.51	5.59	5.37	4.82	3.78	3.11	2.15	1.42	0

Table 5 Tested shear strength of steel under biaxial stress (normal and shear stress)

Specimens	$\mathbf{D_{cs}}$	$\boldsymbol{t_{cs}}$	**H**	$\boldsymbol{f_u}$	$\boldsymbol{f_{cu}}$	$\boldsymbol{N}$	$\boldsymbol{\sigma_{le}}$	$\boldsymbol{\sigma_{le}/f_u}$	$\boldsymbol{T_u}$	$\boldsymbol{\tau_{si}}$	$\boldsymbol{\tau_{si}/f_u}$	
	(mm)			N/mm^2		kN	N/mm^2		kN. m	N/mm^2	Test	Theory
C-T1[a]	ϕ 200.0	6.2	475	481.2	51.2	0	0	0	134.0	328.9	0.68	0.577
C-T2[b]	ϕ 220.2	6.2	1100	465.0	57.9	0	0	0	134.9	285.8	0.62	0.577
C-T3[c]	ϕ 139.8	3.5	1000	459.6	31.2	0	0	0	33.4	299.1	0.65	0.577
C-T4[c]	ϕ 139.8	4.5	1000	426.8	33.0	0	0	0	40.1	280.8	0.66	0.577
C-CT1[b]	ϕ 220.3	5.9	1100	465.0	49.4	700.5	18.4	0.04	144.8	291.8	0.63	0.577
C-CT2[d]	ϕ 101.4	1.55	609.6	315	35.0	89.0	11.02	0.03	5.67	181.78	0.607	0.577
C-CT3[d]	ϕ 101.4	1.55	609.6	315	35.0	151.2	18.73	0.06	5.61	181.62	0.596	0.577
C-CT4[d]	ϕ 101.4	1.55	609.6	315	35.0	249.0	30.85	0.10	5.14	181.21	0.579	0.575
C-CT5[d]	ϕ 101.4	1.55	609.6	315	35.0	302.5	75.15	0.24	4.29	177.94	0.544	0.565

[a] Test results from Yu-Hang Wang et al. [21]; [b] test results from Yu-Hang Wang [5]; [c] test results from Beck J [9]. $\mathbf{D_{cs}}$—diameter of specimen; $\boldsymbol{t_{cs}}$—thickness of circular steel tube; H—height of specimen; f_u —tension strength of steel; f_{cu} —compression strength of concrete; N—axial force applied to specimen; σ_{le}—normal stress of steel; T_u—tested torsional capacity of CFST column; τ_{si}—tested shear strength of steel on normal and shear stress using the Eq. (19)